Vibroacoustic Optimization of Anti-Tetrachiral and Auxetic Hexagonal Sandwich Panels with Gradient Geometry

Mostafa Ranjbar[1,2,*], Luca Boldrin[2], Fabrizio Scarpa[2,3], Simon Neild[3], Sophoclis Patsias[4]

[1]Department of Mechanical Engineering, Eastern Mediterranean University, TRNC via Mersin 10, Turkey
[2]Advanced Composites Centre for Innovation and Science (ACCIS), University of Bristol, BS8 1TR, Bristol, UK
[3]Dynamics and Control Research Group, University of Bristol, BS8 1TR Bristol, UK.
[4]Mechanical Methods, Rolls-Royce plc, PO Box 31, DE24 8BJ Derby, UK

E-mail: mostafa.ranjbar@ bristol.ac.uk , luca.boldrin@bristol.ac.uk, f.scarpa@bristol.ac.uk, simon.neild@bristol.ac.uk, sophoclis.patsias@rolls-royce.com (*Corresponding author)

Abstract

The work describes the vibroacoustic behavior of anti-tetrachiral and auxetic hexagonal gradient sandwich panels using homogenized finite element models to determine the mechanical properties of the auxetic structures, the natural frequencies and radiated sound power level of sandwich panels made by the auxetic cores. The mechanical properties and the vibroacoustic behavior of auxetic hexagonal sandwich panels are investigated as a benchmark. The radiated sound power level of the structure over the frequency range of 0 to 1000 Hz is minimized by modifying the core geometry of the gradient auxetic sandwich panels. Several excitation cases are considered. First-order and random optimization methods are used for the minimization of radiated sound power level of the structures. The results of this study present significant insights into the design of auxetic structures with respect to their vibroacoustical properties.

Keywords: auxetic; anti-tetrachiral; hexagonal; gradient; sandwich panel; vibroacoustic; optimization.

1. Introduction

Cellular structures have lightweight characteristics with significant tuneable mechanical properties [1], and are used in a wide range of aerospace, automotive and general transport applications [2, 3]. Honeycomb structures are a typical and common example of cellular core configurations [4]. Over-expanded centresymmetric cellular configurations can also be developed by internal geometry modification of their cell wall aspect ratio and cell angle [4, 5]. Classical honeycombs exhibit anticlastic curvatures when subjected to out-of-plane bending [6-8], increasing therefore the manufacturing complexity of sandwich structures that posess geometries departing from the rectangular one [9]. To this end, negative Poisson's ratio solids [7] (also known as auxetics) can be used to produce dome-shaped surfaces because of their synclastic curvature, and show at the same time a series of interesting multifunctional properties , [10-12]. Lim has recently presented an overview about auxetic materials and structures, including a brief survey related to the vibration and the acoustic properties of auxetic solids from late 1980s to end of 2014 [13].

Hexagonal centresymmetric honeycombs with negative internal cell angles are not the only example of auxetic cellular structures. Between the different microstructure topologies that possess a negative Poisson's ratio behavior, the chiral honeycomb configuration is an example of geometry that has received significant attention within the cellular materials community. Chiral honeycombs are effectively micropolar materials with in-plane Poisson's ratios close to -1,

showing at the same time a substantial decoupling between the transverse shear and flatwise compressive properties [14-16]. For a view on the mechanics of various chiral honeycomb configurations that Reader can refer, for example, to the work of Grima and co-workers [17]. As an example of application of chiral structures in vibroacoustics, Ma *et al*. have used anti-tetrachiral cellular platforms to host metal rubber particles as a nonlinear metamaterial damper to reduce the level of vibration of a structure [18].

Lim has pioneered the concept of cellular structures with gradient topology in his 2002 seminal work [19]. The microstructure configurations cited above tessellate periodically in the plane, and therefore create cellular panels with assemblies of cells having equal geometry in any location of the structure. However, it is possible to produce cellular panels with gradient configurations, in which the structure is made by a continuous distribution of unit cells with compatible geometry but a single variable parameter (like the internal cell angle or aspect ratio). Scarpa and Tomlinson were between the first to study the vibration characteristics of re-entrant honeycombs [20]. Scarpa et al. also investigated the acoustic properties of auxetic open cell resilient polyurethane foams [21]. These papers (and other produced by different research teams) contributed to the creation of a later body of research about the vibration and the acoustics of auxetic solids.

In a separate work, Lira et al. have adopted a gradient cellular core with auxetic configurations to design aeroengine fan blades with optimized modal mass displacements [22]. Gradient auxetic cores have also been evaluated to engineer damage tolerant sandwich panels and static indentation [23]. Very recent work on the vibration of auxetic plates has also been performed by Maruszewski et al. [24], and by Lim [25]. Ruzzene and Scarpa also investigated the wave propagation in sandwich panel plates with periodic auxetic core [26]. Furthermore, Airoldi et al. presented a work related to the application of chiral topologies to composite morphing aerostructures designs [27]. The periodic and gradient trichiral configurations have been evaluated as dynamic impedance absorbers in vibration transmissibility applications [28].

The numerical optimization of structures versus various acousto-structural properties (such as root mean square level of the structural velocity, radiated sound power) is an integral part of the design of passive noise control structures. A survey of methods and applications of structural acoustic optimization for passive noise control can be found in the review paper by Marburg [29]. Auxetic cellular cores and their gradient versions may offer some significant tailoring of their mechanical and density properties, through the geometry of their unit cells and selection of specific core materials. They may therefore constitute a suitable platform to design structural panels with optimized mechanical and vibroacoustics performance over a range of frequency bandwidths.

This paper is focused on the evaluation of the vibroacoustics response of sandwich panels with auxetic anti-tetrachiral and hexagonal cores in gradient configurations. The radiated sound power level of these auxetic sandwich panels has been minimized with respect to their core geometries. In the following sections, the mechanical behavior of anti-tetrachiral and hexagonal cores is firstly investigated using a numerical homogenization. Also, the minimization of radiated sound from such structures is intensively reported. The paper is organized as follows. The mechanical properties of anti-tetrachiral auxetic core are first introduced, followed by presentation of the modelling and vibroacoustic optimization of anti-tetrachiral gradient auxetic sandwich panel for various loading conditions. A similar modeling approach is also applied to

the auxetic hexagonal sandwich panel model. Final conclusions about the importance of these results are discussed at the end of the paper.

1. Mechanical properties of the anti-tetrachiral auxetic core

An analytical model has been used to calculate the mechanical properties of anti-tetrachiral lattices. Figure 1 shows a typical panel with a Representative Unit Cell (RUC) of the anti-tetrachiral lattice.

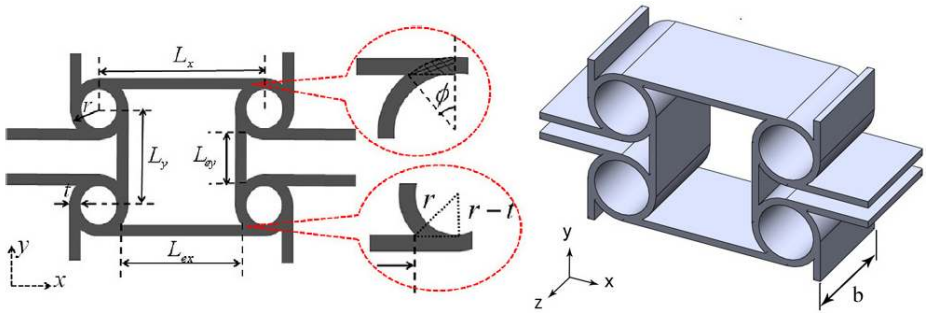

Figure 1. Anti-tetrachiral plate and its representative unit cell [30]

Chen et al. [30] have developed an analytical approach based on strain energy methods to calculate mechanical properties of the anisotropic anti-tetrachiral lattice. The in-plane mechanical properties of these anti-tetrachiral lattices can be defined using four non-dimensional parameters:

$$\alpha_x = \frac{L_x}{r},\ \alpha_y = \frac{L_y}{r},\ \beta = \frac{t}{r},\ \gamma = \frac{b}{r} \tag{1}$$

The in-plane Poisson's ratios and uniaxial moduli E_x, E_y and E_z can be formulated on the basis of these nondimensional parameters and the material properties of the core (Young's modulus E_c and density ρ_c). For details of these formulas please refer to [30]. The shear modulus is particularly important for the mechanics of sandwich structures. Theoretically, the transverse shear modulus of general honeycomb structures is limited within an upper (Voigt) and a lower (Reuss) bound. Those bounds can be obtained by using the theorems of the minimum potential and minimum complementary energies [30]. Lorato et al. have to this end [31] proposed the formula for the calculation of the lower bound for the transversely isotropic lattice. In this work the formulations described in References [30] and [31] are adopted for the homogenization approach of the core.

3. Modeling of the anti-tetrachiral gradient (ATG) sandwich panel

An anti-tetrachiral gradient (ATG) plate is defined by the constant dimension L in the x and y directions, but possesses various cell radiuses (Figure 2).

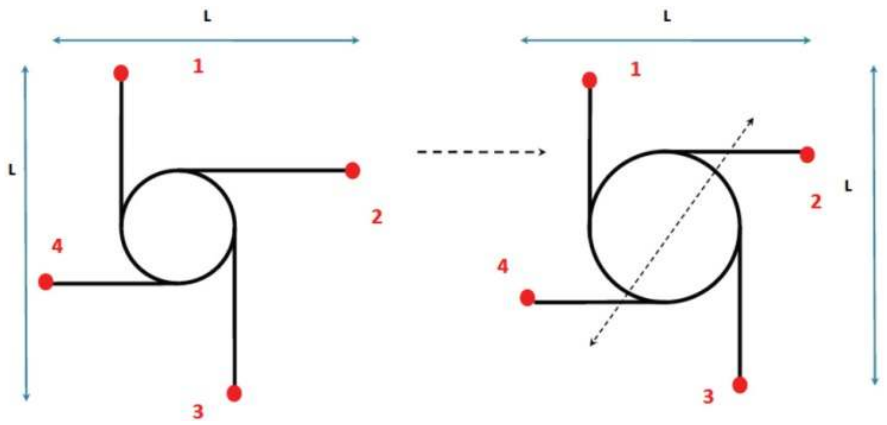

Figure 2. Gradient geometry for the unit cell with varying radius and constant length L

In gradient-shaped structures, the mechanical properties can be modeled as a continuous function distributed over the length of the panel. The equivalent mechanical properties are however function of the relative size between the cell dimensions and the width of cell assemblies having the same cell parameters [28]. The geometry of the original ATG plate configuration is replaced by an equivalent orthotropic material using a compliance matrix [S] defined in [4], and mechanical properties defined in [30] and [31]. The out-of-plane Poisson's ratios υ_{xz} and υ_{yz} are assumed to be near zero, consistently with the assumptions of the Cellular Material Theory [4]. Similarly, the other transverse Poisson's ratios are assumed to satisfy the relation $\upsilon_{zx} = \upsilon_{zy} \approx \upsilon_c$ where υ_c is the Poisson's ratio of the core material [4].

Figure 3.a shows an example of the sensitivity exhibited by the in-plane modulus along the x direction with respect to the radius of a single antitetrachiral unit cell. In this figure, only one anti-tetrachiral cell is considered. The Young's modulus has been normalized against the tensile modulus of the core material E_{ABS}, which is represented by acrylonitrile butadiene styrene (ABS) [30]. As the radius of the nodes increases, the longitudinal stiffness has a decrement proportional to r^{-1}.

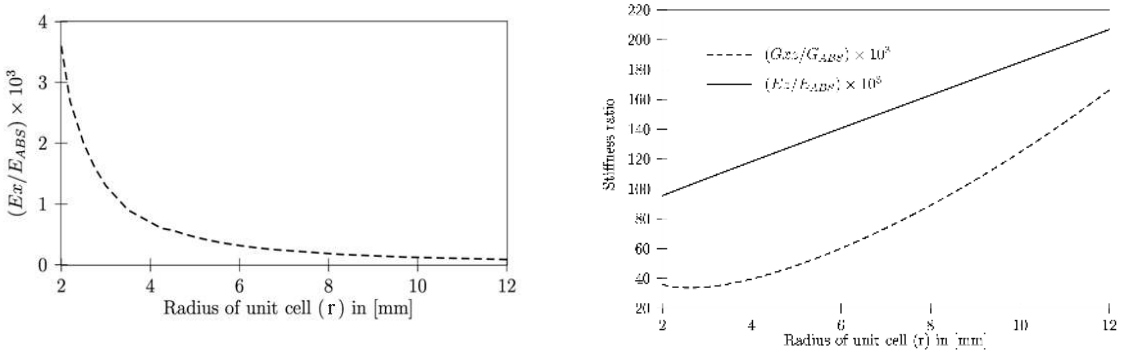

(a) (b)

Figure 3. Variation of in-plane Young's modulus ratio in x direction (a), and transverse shear stiffness G_{xz} or G_{yz} and out-of-plane stiffness E_z (b) with respect to the radius of a single antitetrachiral cell with fixed dimension as $L_x = L_y = 24$ mm, $t = 1$mm and $b = 12$mm

Figure 3.b shows the out-of-plane stiffness E_z is linearly dependent over the radius of the nodes r. The out-of-plane Young's modulus scales as the density of the honeycomb structure [4, 30]. Also, this figure shows the variation of out-of-plane transverse shear stiffness G_{xz} or G_{yz} with respect to r. For increasing values of the radius of the nodes, the out-of-plane shear modulus has a nonlinear behavior, with an initial minima and a steep increase at higher values of r. Theoretically, the transverse shear modulus of general centresymmetric and chiral honeycomb structures is limited within an upper (Voigt) and a lower (Reuss) bound [30]. Those bounds can be obtained by using the theorems of minimum potential energy and minimum complementary energy. For isotropic regular hexagonal lattices, the upper bound does coincide with the lower bound. Although anti-tetrachiral isotropic honeycombs are in-plane isotropic, two different bounds for the transverse shear modulus exist. In this case, G_{xz} and G_{xz} are a nonlinear function of r [31].

3.1 Homogenization of FE model for auxetic sandwich panel

To perform the modal analysis for the anti-tetrachiral sandwich panel with the uniform cell distribution the ANSYS Rel. 11.0 commercial FE analysis package has been used [32].

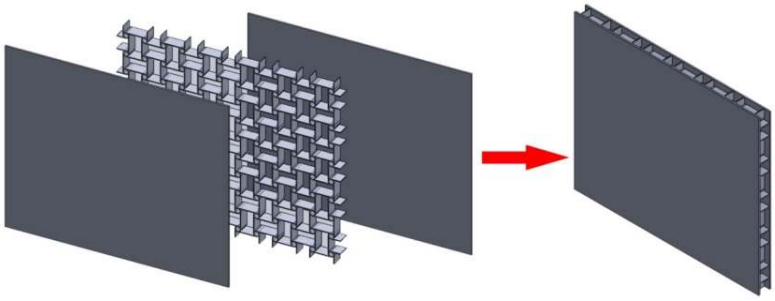

Figure 4. Full scale sandwich panel with anti-tetrachiral auxetic core

Figure 4 shows a full scale sandwich panel model with a core made from 6×5 anti-tetrachiral unit cells. The skins of the sandwich make two $288\times240\times2$ mm plates. The geometry parameters of the anti-tetrachiral core are listed in table 1. The elastic properties of the core material, i.e. ABS, are considered from Ref. [22]. As indicated by Alderson *et al*. for anti-tetrachiral systems [2,3], the in-plane Poisson's ratio calculated through finite element (FE) modeling and experimental analyses provide a similar result (-0.98), and in general show a quite good correlation between simulations and test data. The compliance matrix [S] typical of centresymmetric honeycomb structures [4] is used to represent the asymptotic homogenized mechanical properties, with the engineering constants from [2, 3, 30, 31] and $\upsilon_{xy}=-0.98$ used for the in-plane Poisson's ratio.

Table1. Geometrical parameter values of the core of sandwich panel

Parameter	r	L_x	L_y	t	b
Value in [mm]	4	24	24	1	12

The application of unit cell homogenization in the calculation of the vibroacoustic behavior of auxetic structures has been already proposed by Chekkal *et al.* [33]. The homogenization of the sandwich plate is performed by using shell elements to represent the skins, while the homogenized core of the anti-tetrachiral cells is represented by two solid element per gauge thickness, with their properties defined by the compliance matrix [S] (Fig. 5). This homogenized structure represents a single core unit cell-two skins unit, which is then propagated as solid and FE model along the two x and y directions to make the full-scale sandwich panels with overall dimensions cited above.

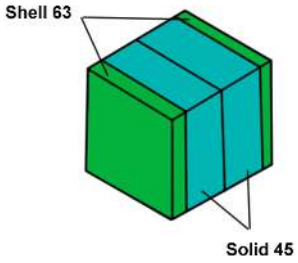

Figure 5. The FEM sample of a homogenized auxetic sandwich panel with SHELL63 elements for its skins and two SOLID45 elements per gauge thickness in its core

To find the appropriate finite element types for the modelling and the homogenization of the auxetic sandwich panel a sensitivity analysis on the full-homogenized model is done with respect to its natural frequencies. At this regard, various element types are considered for the modelling of skin and core of auxetic sandwich panel. Element like SHELL63 for the skin and SOLID45 have been selected after this benchmark. The modal performance of the full-scale homogenized model is then compared against the one of a full scale FE model that represents the detailed geometry of the core and the skin of the panel (Figure 4). In the full-scale detailed model both face skins and the cells are represented by SHELL63 elements, with constant elements size equal to $b/4$, corresponding to a minimum length of 12 mm has been selected for the elements after a convergence tests on the first five modes. The skins and the cell walls were modeled using the ABS plastics material properties. Both in the homogenized and full-scale detailed FE models the simply supported boundary conditions have been applied by clamping the translational degrees of freedom (DOF) u_x, u_y and u_z at nodes located at the geometric half-plane of the core [34]. These nodes are located on the neutral plane of the sandwich, and correspond in the homogenized model to the geometric half of the core when two solid elements per core thickness are adopted.

Table 2 shows the natural frequencies of the ATG sandwich panel for the homogenized and full scale FE sandwich panels. The sandwich panel exhibit the classical (m,n)-type of flexural modes, with the peculiarity that the (2,2) modeshape has a lower frequency than the (1,3) one. Furthermore, the homogenized model shows to be an excellent approximation to the full-scale finite element representation. These results confirm the degree of fidelity that the homogenized core approach provides for the analysis of the modal behavior of sandwich panel ruled by flexural modeshapes.

Table 2. Natural frequencies of Anti-tetrachiral sandwich panel on the frequency range of 0 to 1000 Hz for the homogenized and full scale FE models

Frequency (Hz)	Model type	Mode 1	Mode 2	Mode 3	Mode 4	Mode 5
	Homogenized	285.23	572.13	687.82	894.61	956.24
	Full scale FE	285.71	572.45	688.02	895.13	958.12

Two different loading conditions (Figure 6) are considered to excite all the modes of the model within a frequency range covering the first five global modes, and this is represented by.the non-symmetric harmonic pressure excitation at z direction, as previously proposed by Ranjbar *et al*. [35] is considered. The pressure loadings in the various areas are all in phase and have the same amplitude. Figure 6 also shows in clearer terms the distribution of homogenized anti-tetrachiral unit cells with same assembled to each other and forming the whole sandwich panel. The gradient (or graded) cell distribution is composed by five distinct regions (R_1, R_2, R_3, R_4, R_5). Each region is shown with a different color.

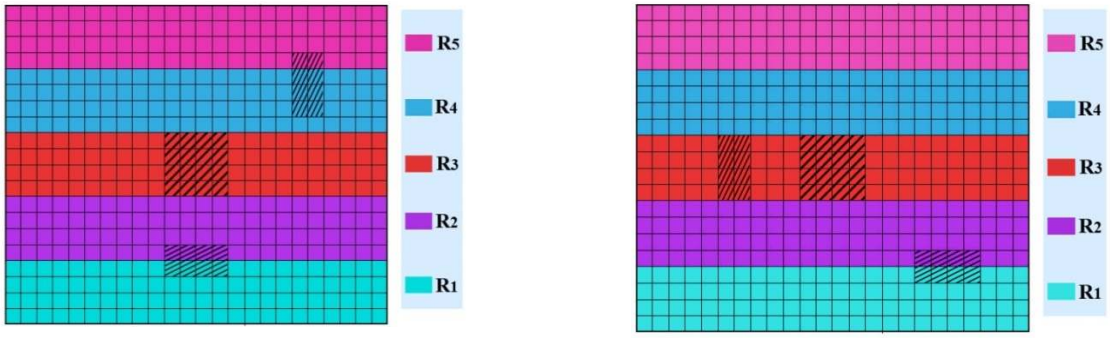

(a) (b)

Figure 6. Various external pressure loadings (dashed areas) on the homogenized FEM of auxetic sandwich panel regions with different core cell radiuses R_1 to R_5.

In next section, the dynamical behavior of the auxetic sandwich anti-tetrachiral panel model will be investigated. The main objective is to determine the radiated noise from the model. Then, the geometry of model will be modified to reduce the radiated noise.

4. Vibroacoustic optimization of the ATG sandwich panel

In this section, the minimization process of the radiated sound power level over the frequency range of 0 to 1000 Hz is discussed. In this regard, the objective function for the optimization process is the root mean square level of radiated sound power level (RMSL) of the ATG model. Here, the radiuses of the unit cells are considered as the design variables. The general optimization problem is defined as:

$$\text{Minimize RMSL}(R_1, R_2, R_3, R_4, R_5) \text{ when } 3mm \leq R_1, R_2, R_3, R_4, R_5 \leq 9mm \quad (2)$$

In the following subsection the calculation of the RMSL is presented, followed by the discussion of the optimization of the model with respect to its vibroacoustics performance.

4.1 Calculation of the radiated sound power

A good metric to quantify the emitted noise from a structure or a machine part is the level of radiated sound power $L_p(f)$, or sound power level for short, defined as:

$$L_s(f) = 10 \times \lg \frac{P(f)}{P_0}, \tag{3}$$

Where $P(f)$ is the radiated sound power and P_0 = 10^{-12} W is a standardized reference value. Here f is the frequency (in Hz). The radiated sound power $P(f)$ can be calculated as [36]:

$$P(f) = \rho_a c_a S \overline{v^2_{\perp rms}}(f) \sigma(f). \tag{4}$$

The parameters ρ_a $[kg/m^3]$ and c_a $[m/s]$ are the density and the speed of sound of the surrounding fluid (in this case air), respectively. Also, S is the area of the sound-radiating surface in $[m^2]$, $v^2_{\perp rms}(f)$ is the mean squared normal velocity of the surface averaged over the radiating surface, and $\sigma(f)$ is the radiation efficiency factor. The quantity $Z_a = \rho_a c_a$ is the so-called specific impedance of air. Fritze *et al.* [37] indicated that for exterior acoustics the solution of the fluid part of the structural acoustic problem is the 'bottle-neck' during the optimization process because of the large computing times required for this part of the analysis. This remark is valid for fluid structure interaction problems, as well as for one-way coupled sequential evaluations, i.e. when the structure excites the fluid but the fluid does not act back on the structure. Several methods are known to circumvent the solution of the acoustic boundary value problem, but because of the intrinsic simplicity and efficiency of calculation the radiated sound power L_s can be approximated by the equivalent radiated sound power (ERP) [36] when the radiation efficiency is set to be 1.0. The ERP does not contain any local acoustic effect, since all sources (herein: all finite elements) have the same radiation efficiency of σ = 1. Therefore, the ERP will usually overestimate the radiation, but will however give a qualitatively good approximation for the structure–induced acoustical fields, especially as an upper bound estimation [37, 38].

The closed analytical solution value of the in-plane shear modulus of the anti-tetrachiral systems has not been determined yet in open literature. To assess the possible effects that the variation of the in-plane shear modulus has upon the radiated sound pressure response of a panel, a FE model is developed based on the original sandwich model (core with SOLID45 elements and skins with SHELL63), but with a linear variation of the shear modulus G_{xy}. The results of the sensitivity of the radiated sound power at the first natural frequency are shown in Figure 7. As it can be observed, the variation of the ERP versus the value of the in-plane shear modulus is negligible, and therefore a first-order shear deformation analysis of sandwich panel is applicable in this case.

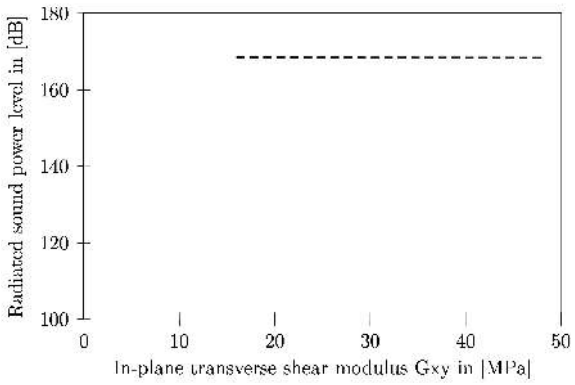

Figure 7. Variation of radiated sound power level with respect to G_{xy} for the ATG sandwich panel

Finally, the mean-squared level of radiated sound power (RMSL in dB) over a frequency range between $f_{\min}$ to $f_{\max}$ can be calculated as:

$$RMSL = \sqrt{\frac{\int_{f_{\min}}^{f_{\max}} L_s^{\,2}(f)\,df}{f_{\max} - f_{\min}}} \tag{5}$$

The RMSL is considered as the objective function to be minimized.

First-order (gradient-based) and random optimization tools of ANSYS are used for the minimization of the RMSL. The random optimization tool calculates the objective function in various randomly selected design points and reports the lowest one as the best optimum result. The first-order method uses derivative information, that is, gradients of the dependent variables with respect to the design variables. It is highly accurate and works well for problems having dependent variables that vary widely over a large range of design space [32]. However, this method can be computationally intense. At the beginning of the iteration the gradient calculations are performed to determine a search direction, and a line search strategy is adopted to minimize the unconstrained problem. The gradients are calculated numerically by finite difference method. The forward difference step, i.e. changes in the radius of auxetic unit cell, is considered to be 0.2%. The maximum number of iterations is considered to be 20.

4.2 Minimization of the RMSL for the ATG sandwich panel

At first, the effect of the thickness variation on the RMSL performance of the ATG sandwich panel with a constant cell radius of 4 mm is evaluated. The results for the two loading cases indicate that the radiated sound power decreases with the increase of the ATG core thickness (Fig. 8). The optimum thickness for the two loading cases is identified to be at 18 mm, while the radiuses of the cells are unchanged during the optimization.

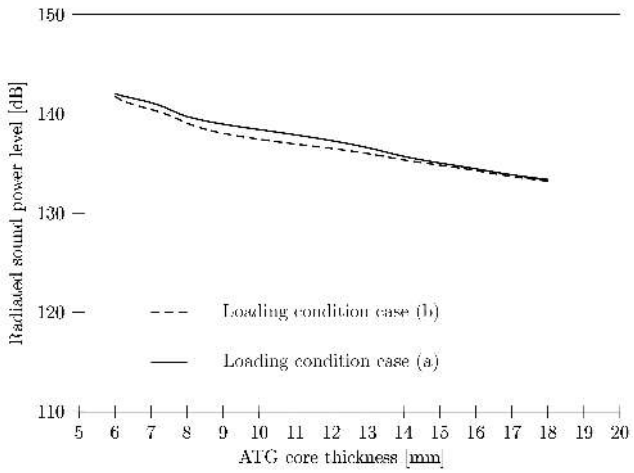

Figure 8. Root mean square of the radiated sound power level with respect to ATG thickness, with constant cell radius of 4 mm

The gradient sandwich plate is considered to be composed of five different sectors with five different radiuses $\{R_1, R_2, R_3, R_4, R_5\}^T$. Each sector is modeled with the homogenized approach (core with SOLID45 elements having the homogenized [S] compliance of the ATG cellular material and SHELL63 skins). Each sector has the compliance matrix calculated with the analytical properties of the anti-tetrachiral core [30], and correction factors taking into account the relative size of the sector and calculated following a procedure indicated in [22]. The skin plate has the same material as the core material. The skin thickness of the plate is uniform and equal to 2 mm. The area geometry of the external skin is 288×240 mm. Both of the skin thickness and the surface dimensions of the skin are fixed.

Table 3 lists the optimization variables and the mass of the sandwich plate for the original, after random optimization and after first order optimization design sets (both excitation cases "a" and "b" when the thickness of plate is fixed). The RMSL for the loading case "a" is reduced to 134.53 dB, while for case "b" the reduction is to 134.28 dB. The mass of the sandwich plate has however increased during the optimization by 11%. The optimization process by first-order method for both loading conditions, "a" and "b", has converged after 50 iterations. The results related to the change of the radiuses in the different regions for the two loading cases shown in Fig. 6 confirm that for the minimization of the radiated sound, larger radiuses of the cells should be considered in all regions of the ATG sandwich panel. It is however worth mentioning that the optimized solutions provide an ~ 11% increase in weight compared to the original design.

Table 3. Optimization results for ATG model under loading cases "a" and "b" after 50 iterations with fixed thickness of plate

	R_1 (mm)		R_2 (mm)		R_3 (mm)		R_4 (mm)		R_5 (mm)		RMSL (dB)		Mass (Kg)	
Loading case	"a"	"b"	"a"	"b"	"a"	"b"	"a"	"b"	"a"	"b"	"a"	"b"	"a"	"b"
Original design	4	4	4	4	4	4	4	4	4	4	137.30	136.52	0.38	0.38
Random method	8.03	7.20	7.59	8.91	7.70	8.51	5.33	6.63	8.63	6.06	134.59	134.42	0.422	0.424

First-order method	6.48	5.80	7.95	8.55	8.61	8.88	6.88	7.23	7.31	7.41	134.53	134.28	0.422	0.424

In figure 9.a, the variation of the radiated sound power level over the frequency range of 0-1000 Hz for the first loading case of Fig. 6 is shown. For these simulations the thickness of the ATG model is unchanged and constant in all parts of the plate. The natural frequencies of the structure with the optimum cell radiuses distribution are shifted to higher values. Also, the last two modal frequencies of the original structure have shifted to the 1010 Hz and 1090 Hz. Figure 9.b shows that by changing the cells radius and the total thickness of model one can obtain the best result for the minimum radiated sound power level.

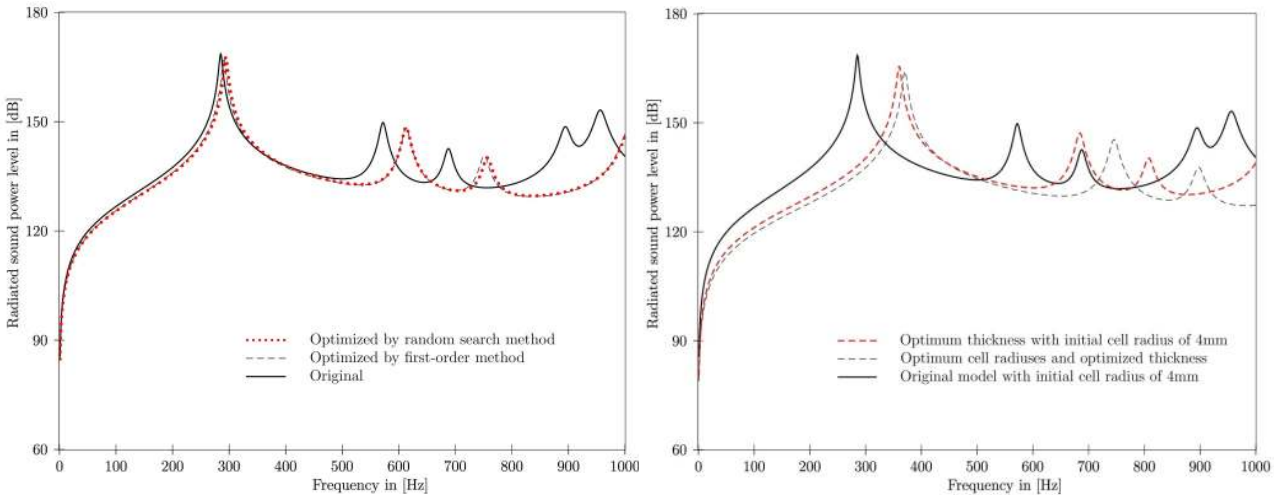

(a). Optimized cell radiuses without any variation in the thickness of panel

(b). Optimized thickness and cell radiuses

Figure 9. Sound power level reduction of ATG model for the loading case “a” shown in figure 6.

Figure 10 shows the optimization results related to the loading case “b”, when the radius of the cells and the thickness of the ATG have simultaneously changed The optimum radiuses distribution shown in table 3 has been obtained by using the first order method. The fundamental natural frequency of the optimum structure is moved to higher values. Also, the number of resonances is decreased within the frequency range between 0 Hz to 1000 Hz.

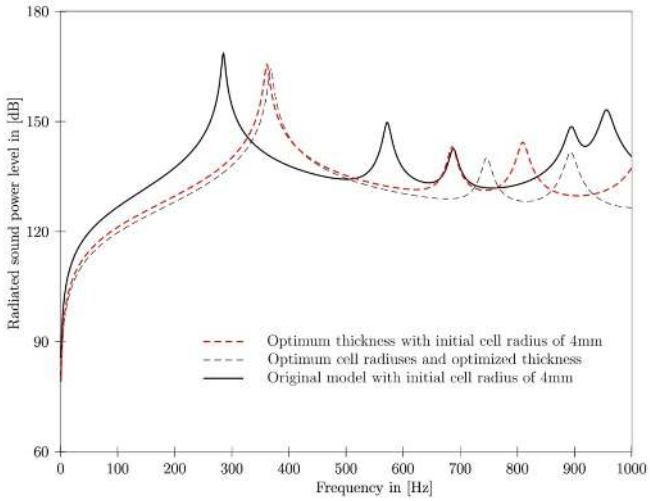

Figure 10. Minimization of the radiated sound power level with respect to the ATG thickness and various cell radiuses (loading condition case "b")

It is important to monitor the mass variation of model after each optimization attempt. For this purpose, the normalized acoustic sound power $(\bar{P})$ can be evaluated as defined by:

$$\bar{P} = P_{acoustics} \Big/ T \tag{6}$$

$$T = \frac{1}{2} M \omega^3 A \tag{7}$$

In equations 6 and 7, T is the kinetic power of structure and $P_{acoustics}$ is the radiated sound power from the model both in Watt. The kinetic power is an indicator of the kinetic mechanical energy of the radiating surface of the sandwich panel in a unit time. The kinetic power can be calculated in term of mass of sandwich panel, the radiating surface area of plate, and the frequency of plate. In Eq. 7 M is the mass of the sandwich panel (in Kg) and A is the surface area of model in [m^2] which is equal with 0.24×0.288. Also, ω is the circular frequency of the harmonic excitation pressure loads in [s^{-1}]. Furthermore, the normalized frequency ω_n is defined in Eq. 8, in which ω_1 is the first fundamental frequency of model.

$$\omega_n = \frac{\omega}{\omega_1} \tag{8}$$

The reduction of the normalized radiated sound power level with respect to thickness and radius variation for the two loading cases "a" and "b" are presented in table 4. The normalized fundamental resonances for both cases "a" and "b" are shifted to higher frequencies, and the value of the optimum normalized sound power calculated by first-order optimization methods is also significantly decreased. For the optimum thickness and ATG cell radiuses case of loading "a", the normalized frequency has increased by 30%, and the normalized radiated sound power decreased by 88.1%. Furthermore, for the optimum thickness of 18 mm and constant radius of 4

mm the normalized frequency has increased by 26% and the normalized radiated sound power decreased by 81.73%. In the loading case "b" when optimum thickness and optimum ATG cell radiuses distributions are considered, the normalized frequency has increased by 29% and the normalized radiated sound power is decreased by 86.11%. When the optimum thickness and constant radius of 4 mm are however considered the normalized frequency decreases by 26.5% and the normalized radiated sound power is diminished by 80.41%. Table 4 shows that for the two loading cases the structures with the optimum thickness and radius have in general the larger normalized frequencies and the smallest normalized radiated sound power.

Table 4. Reduction of normalized radiated sound power for ATG model

Loading condition	Model	Normalized frequency ω / ω_1	Normalized radiated sound power $\times 10^5$
Case "a"	Constant thickness and radius	1	94.7
	Optimum thickness and radius	1.30	11.2
	Optimum thickness, constant radius	1.26	17.3
Case "b"	Constant thickness and radius	1	96.5
	Optimum thickness and radius	1.29	13.4
	Optimum thickness, constant radius	1.265	18.9

5. Modelling the auxetic hexagonal sandwich panel

In this section, the mechanical and vibroacoustic properties of the auxetic hexagonal sandwich panel are analysed.

5.1 Mechanical properties of auxetic hexagonal sandwich panel

The sandwich panel with auxetic hexagonal consists of 15×10 auxetic hexagonal unit cells with negative internal angle of $\theta = -20^{\circ}$. The total dimension of the plate is 288×240 mm. To keep the first natural frequency of the auxetic hexagonal sandwich panel same as the one of the ATG sandwich panel, the geometry of the model is as given in table 6. In figure 11, a single cell of the auxetic hexagonal sandwich panel and its geometrical parameters are shown.

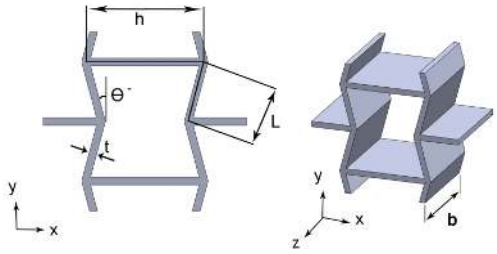

Figure 11. A representative unit cell of the auxetic hexagonal cellular structure

Table 5 shows the geometrical parameters of the original model related to the auxetic the auxetic hexagonal sandwich panel.

Table 5. Geometrical parameters of auxetic hexagonal sandwich panel

h (mm)	l (mm)	t (mm)	b (mm)	θ (degree)
16.77	8.51	1	10.23	-20

Figure 12.a shows a gradient hexagonal cellular configuration along the x direction. The generation of the gradient core is performed from the base hexagonal unit as shown in figure 12.b, which is defined by the constant dimension L_1. Each section of the band-graded core has six geometrically fixed points 1-6, while the geometry of each region changes with change in angle θ. The lengths h and L can be calculated using the formula proposed by Lira *et al*. [22]

(a)

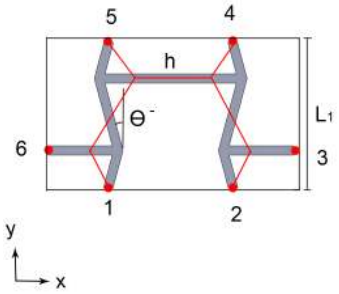

(b)

Figure 12. (a). Hexagonal gradient core [19], (b). Gradient geometry for the unit cell with varying angles and constant length L_1 (from [22])

For simplicity, the gradient core has also been in this case replaced by an equivalent special orthotropic homogenized material with a suitable compliance matrix [S] [22]. The out-of-plane Poisson's ratios υ_{xz} and υ_{yz} are assumed to be zero, consistently with the assumptions of the cellular material theory [4]. Similarly, the other transverse Poisson's ratios are assumed to satisfy the relation $\upsilon_{zx} = \upsilon_{zy} \approx \upsilon_c$ where υ_c is the Poisson's ratio of the core material [4]. The formulations given by Gibson and Ashby [4] for the mechanical properties of honeycombs are valid only for infinite honeycombs, typically for panels made of 12×12 cells or above [22]. For structures made of periodic assemblies of fewer cells, it is possible to observe a general decrease of stiffness, accompanied by variations of the Poisson's ratio from the theoretical infinite panel solution [19]. While 10×10 honeycomb panels show substantially the same behavior under uni-axial tensile loading (i.e., the E_x and E_y moduli are the same), a 2×10 cell panel will have a decreased stiffness E_x compared to the one predicted by the theoretical analysis [22]. In table 6, the finite element results for a 2×10 auxetic hexagonal core and 4×10 auxetic hexagonal core for both angles $\theta = -20^{\circ}$ and $\theta = -30^{\circ}$ are shown. A 2×10 cell panel will have a stiffness E_x substantially decreased compared to the analytical prediction, but a 4×10 core with two rows at $\theta = -20^{\circ}$ and two rows at $\theta = -30^{\circ}$ will yield an equivalent stiffness closer to the one predicted by the analytical formulas.

Table 6. Theoretical and finite element model values for E_x of auxetic hexagonal core

Cell angle θ	Theoretical value from ref. [4]	Calculated FEM value	Calculated FEM value

in degree	for 10×10 core	for 2×10 core	for 4×10 core
-20	5.58 Mpa	1.48 Mpa	4.24 Mpa
-30	5.14 Mpa	1.40 Mpa	4.10 Mpa

Table 7 also shows that for a 8×10 gradient cell panel consisting of 4 rows of auxetic cells at $\theta=-20^{\circ}$ and 4 rows of units at $\theta=-30^{\circ}$ will have mechanical properties close to the theoretical values. Therefore for gradient cell cores greater than 8×10, the theoretical value predicted for E_x can be considered an adequate approximation.

Table 7. Theoretical and FE results for the E_x modulus of auxetic hexagonal gradient core

2-Layered gradient configuration	Average theoretical from *Ref.* [4]	Calculated by FEM	Average by FEM (2 separate layers)
4×10 (2×10, θ=-20° and 2×10, θ=-30°)	5.36 Mpa	4.24 Mpa	1.44 Mpa
8×10 (4×10, θ=-20° and 4×10, θ=-30°)	5.36 Mpa	5.41 Mpa	4.16 Mpa

5.2 FE modelling of auxetic hexagonal sandwich panel

Similarly to the other models so far developed, the plate skin is modeled with SHELL63 elements and the core with SOLID45 ones containing the homogenized material. The natural frequencies of the auxetic hexagonal sandwich are given in table 8.

Table 8. Natural frequencies of sandwich panel with auxetic hexagonal core

Mode	1	2	3	4	5
Frequency (Hz)	285.14	557.15	844.21	928.02	1031.90

For the harmonic analysis of the auxetic hexagonal sandwich panel, simply supported boundary conditions by constraining the translational degrees of freedom in the neutral plane of model are considered. The same excitation cases used for the ATG model are also considered. The applied pressures are in the frequency range between 0 Hz and 1000 Hz.

In figure 13.a, the variations of both E_x / E_{ABS} and E_y / E_{ABS} with the variation of the angle θ are shown, with E_{ABS} being the Young's modulus of the core material (ABS plastics). The graphs show that with an increase in angle θ, E_x slightly increases, but the increment of E_y is more significant. Also the out-of-plane Young's modulus E_z is decreased when the angle θ is increased [4].

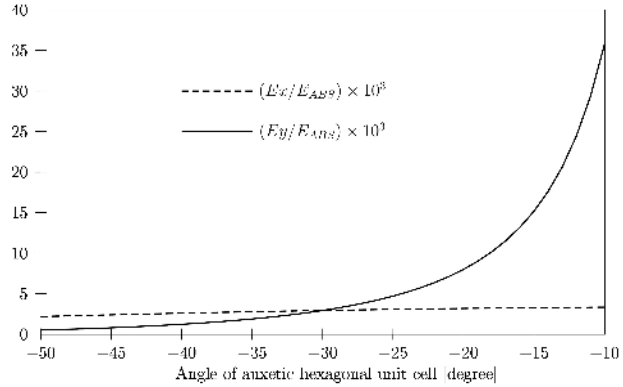

(a). In-plane young modulus ratios

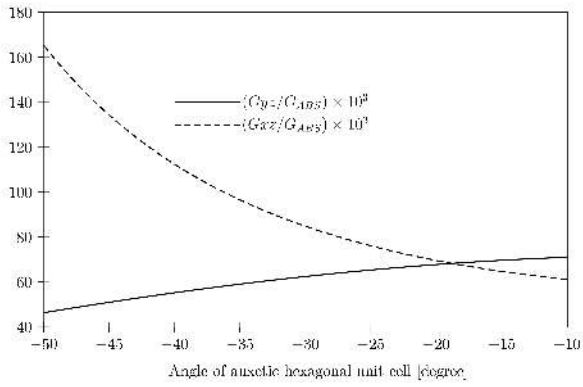

(b). Out of plane transverse shear stiffness G_{xz} and G_{yz}

Figure 13. Variation of mechanical properties of a single auxetic hexagonal cell

Figure 13.b depicts variation of out-of-plane transverse shear stiffness G_{xz} and G_{yz} with change of cell angle, while the thickness of the core is 10.23 mm.. With an increase of the cell angle, G_{xz} decreases and G_{yz} increases respectively. Also in this case (and similarly to the ATG panel) the sensitivity of the radiated sound power level is negligible with respect to G_{xy}. Figure 13.a indicates that the in-plane Young's moduli of a single auxetic hexagonal cell have in general larger values when the cell angle is small (in magnitude). However, the moduli will tend to decrease with respect to the cell angle from -10 to -30 degrees, while after these angle values no significant changes in uniaxial stiffness are noticeable. This trend is totally different for the out of plane transverse shear stiffness (Figure 13b), and for a cell angle of -30^{o} the two transverse moduli differ substantially. These observations can give a guideline to design hexagonal auxetic structure cell angles when a specific loading case, e.g. bending or torsion, should be considered.

5.3 Minimization of RMSL for auxetic hexagonal sandwich panel

5.3.1 Optimizing the angle of the hexagonal sandwich panel

The auxetic hexagonal gradient plate is considered to be composed of five different sectors with five different negative angles $\{\theta_1,\ \theta_2,\ \theta_3,\ \theta_4,\ \theta_5\}^{T}$. The skin plate has the same material as the core material and the thickness of the skin is fixed. First-order and random optimization ANSYS routines are used for the minimization of the RMSL. Figure 14 shows the change of the angles in different regions during the optimization iterations for the load case "a".

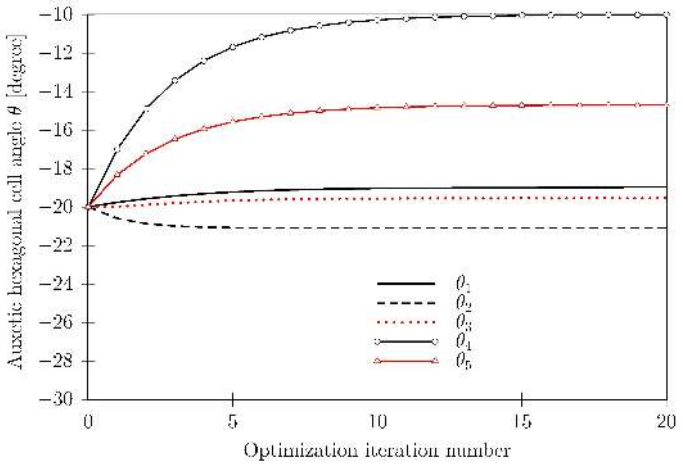

Figure 14. Change of the hexagonal auxetic cell angle during the optimization by using the first order method for the first loading condition (Fig. 6.a).

In table 9, the optimization results for the minimization of the radiated sound power level of auxetic hexagonal sandwich panel with constant thickness are shown.

Table 9. The optimization variables for the auxetic hexagonal sandwich panel under loading cases "a" and "b" after 20 iterations

	θ_1 (Degree)		θ_2 (Degree)		θ_3 (Degree)		θ_4 (Degree)		θ_5 (Degree)		RMSL (dB)		Mass (Kg)	
Loading case	"a"	"b"	"a"	"b"	"a"	"b"	"a"	"b"	"a"	"b"	"a"	"b"	"a"	"b"
Original design	-20		-20		-20		-20		-20		135.89	135.52	0.399	0.399
First-order method	-18.99	-18.51	-21.09	-18.25	-19.54	-16.11	-10.02	-10.01	-14.71	-15.02	135.17	134.44	0.397	0.396
Random search method	-45.74	-14.64	-23.56	-27.32	-17.75	-21.10	-13.51	-11.11	-20.39	-10.65	135.53	134.69	0.398	0.397

For the load case "a", the root mean square of the sound power level is reduced by 0.72 dB, and by 1.08 dB for the load case "b". Figures 15.a and 15.b show the reduction of the sound power level by using various optimization methods when the two loading cases are considered. The first resonance in the spectra related to the "b" case has been shifted to a higher value than for the case "a". It is noticeable that in both cases the radiating peaks related to the 3rd and 4th global modes are reduced and shifted to higher frequency values within the same frequency range. This behavior appears to be essentially stiffness dominated, because the mass for the optimized configurations changes in a very negligible way compared to the original design (Table 9).

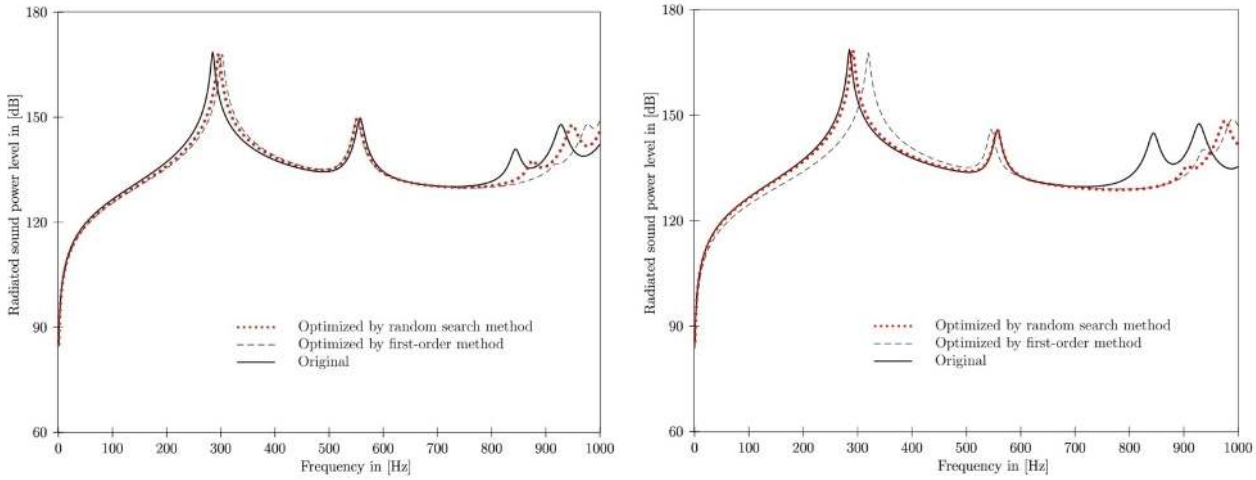

(a). loading case "a" (b). loading case "b"

Figure 15. Sound power level reduction for the auxetic hexagonal panel

5.3.2 Optimizing the thickness of hexagonal sandwich panel

Figure 16 shows the variation of the radiated sound power level for the loading profile "a". The first case has a constant cell angle of $\theta = -20°$ and thickness of 10.23 mm. The second one has constant cell angle of $\theta = -20°$ and the optimum thickness of 18 mm, while the third one has an optimum cell angle that has been derived using the first order method and an optimum thickness of 18 mm. It is clear that the fundamental natural frequency of the optimum structure is moved to higher values in all the cases. Also, the modal density is decreased over the frequency considered for these simulations because of the way the stiffness to mass ratio of the structure has increased.

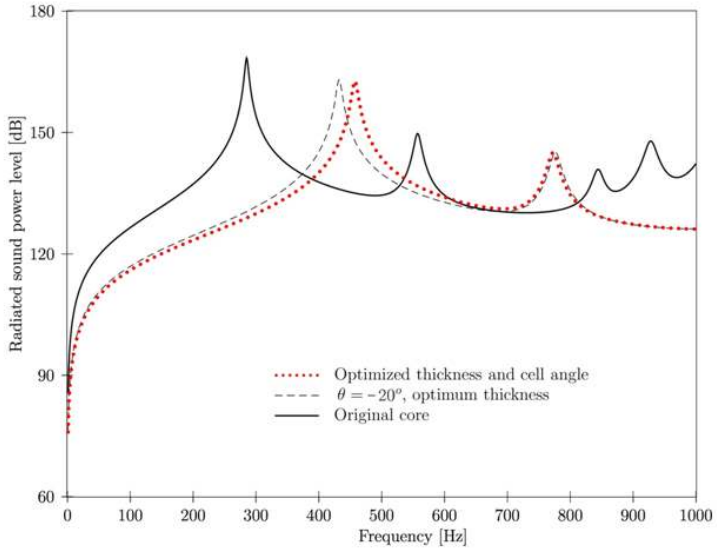

Figure 16. Radiated sound power level minimization for loading case "a"- auxetic hexagonal core thickness optimization

For the loading case “a”, the normalized frequency is increased by 51.5% for the auxetic hexagonal core with a cell angle of $\theta = -20°$ and optimum thickness of 18 mm, and the normalized radiated sound power decreases by 93%. For the case related to both cell angles and thickness being optimum, the normalized frequency increases by 60% while the normalized radiated sound power is reduced by 94.6%. These results are also very similar to the ones observed for loading case “b”. The masses of the auxetic hexagonal sandwich panel corresponding to the pressure load cases “a” and “b” with the optimum cell angles and optimum thickness of 18 mm are 0.480 Kg and 0.478 Kg respectively. In both cases the mass are increased compared to the original configuration.

6. Comparison of the normalized radiated power performance between the auxetic optimized configurations

Figure 17 gives a global comparison of the normalized radiated sound power levels in logarithmic scale of the original and optimized ATG and auxetic hexagonal models for the loading case “a” with respect to the normalized frequency. The figure shows the effect of the gradient geometry on the reduction of the radiated noise from the auxetic sandwich panel, and it generally indicates that the modal density has decreased for the gradient structures within the normalized frequency range.

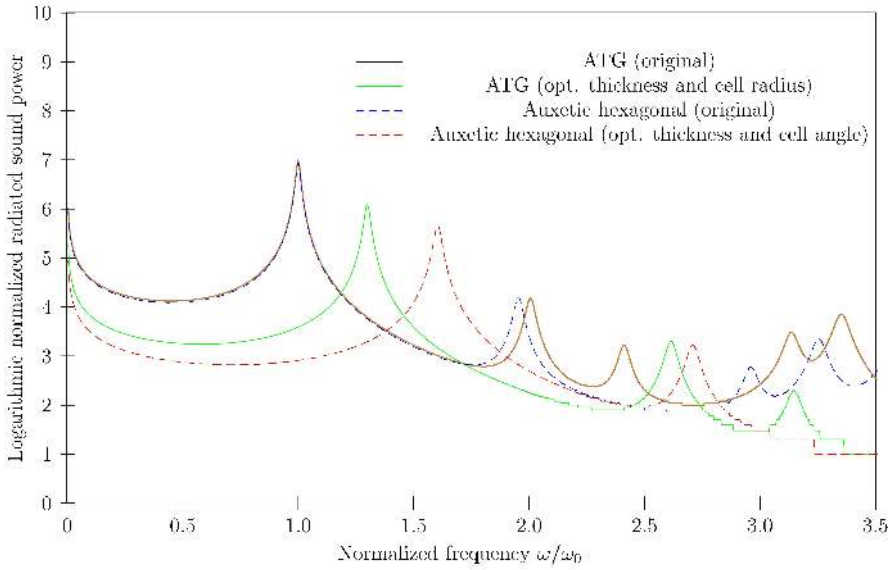

Figure 17. Effect of gradient geometry on reduction of radiated noise in auxetic sandwich panels (loading case “a”)

Compared to the original non-optimized models, it is possible to notice a general reduction of the normalized radiated sound power, and an increase at the same time of the normalized frequency for the first resonance. The auxetic hexagonal model shows the lowest level of radiated noise, in particular for the first peak. Low levels of radiated noises are also observed in the case of the first loading level for the other resonances within the normalized frequency range for the optimized auxetic re-entrant configuration, rather than in the ATG

morphology. At higher frequencies, the optimum models behave fairly similarly, both in terms of modal density and overall sound power levels. The optimum auxetic hexagonal configuration has also the advantage of featuring the lowest amount of mass increment in comparison to the original model, and this is a particularly interesting point in terms of potential applications like airframe structures. It should be emphasized that with the one-dimensional gradient geometry considered in this work one can adjust the mechanical properties of the original material simultaneously along the three Cartesian directions.

7. Conclusions

The paper has described the vibroacoustic behavior of anti-tetrachiral and auxetic hexagonal gradient sandwich panels. A homogenized finite element modeling approach has been used to determine the mechanical properties of the auxetic structures, the natural frequencies and the radiated sound power level of sandwich panels made by the auxetic cores.

Both of the auxetic core geometry and thickness of the sandwich panels affect the radiated sound power level of the structure. In general, the first resonance belonging to the optimized structures shifts towards higher frequencies. Furthermore, the optimized structures radiate a lower level of structure-borne sound.

The location of the excitations plays an important role on the radiated noise level from the structures, both for the ATG and the auxetic hexagonal sandwich panels. Therefore, it is recommended to use the gradient core geometries to cover the excitations areas (see loading case "a").

The auxetic hexagonal model performs better to reduce structure-born radiated noise, especially at low frequency ranges. At higher frequencies however, the optimum configurations of the ATG and auxetic hexagonal sandwiches behave fairly similarly, both in terms of modal density and overall sound power levels. The optimum auxetic hexagonal configuration has also the lowest amount of mass increment in comparison to the original model. This is a feature that could be considered for potential airframe structures applications, in which weight reductions or control are paramount.

Acknowledgement

The authors would like to acknowledge Rolls-Royce plc for the support of this work through the Composites University Technology Centre (UTC) at the University of Bristol, UK. Special acknowledgements go also to the Strategic Investment in Low carbon Engine Technology (SILOET) programme supported by Rolls-Royce plc and Technology Strategy Board (TSB).

References

1- Bitzer, T., 1997, Honeycomb Technology: Materials, Design, Manufacturing, Applications and Testing. Chapman & Hall, London.
2- Alderson, A., Alderson, K., Attard, D., Evans, K., Gatt, R., Grima, J., Miller, W., Ravirala, N., Smith, C., Zied, K., 2010, "Elastic constants of 3-, 4-and 6-connected chiral and anti-chiral honeycombs subject to uniaxial in-plane loading," Compos. Sci. Technol., **70**, 1042–1048.

3- Alderson, A., Alderson, K., Chirima, G., Ravirala, N., Zied, K., 2010, "The in-plane linear elastic constants and out-of-plane bending of 3-coordinated ligament and cylinder-ligament honeycombs," Compos. Sci. Technol., **70**, 1034–1041.
4- Gibson, L.J., Ashby, M.F., 1997, Cellular Solids: Structure and Properties, second ed. Cambridge University Press.
5- Bezazi, A., Scarpa, F., Remillat, C., 2005, "A novel centresymmetric honeycomb composite structure," Compos. Struct., **71**, 356–364.
6- Evans, K., 1991, "The design of doubly curved sandwich panels with honeycomb cores," Compos. Struct., **17**, 95–111.
7- Lakes, R., 1987, "Foam structures with a negative Poisson's ratio," Science, **235**, 1038–1040.
8- Masters, I., Evans, K., 1996, "Models for the elastic deformation of honeycombs," Compos. Struct., **35**, 403–422.
9- Evans, K.E., Alderson, A., 2000b, "Auxetic materials: functional materials and structures from lateral thinking," Adv. Mater., **12**, 617–628.
10- Evans, K., Alderson, K., 2000a, "Auxetic materials: the positive side of being negative," Eng. Sci. Edu. J., **9**, 148–154.
11- Bettini, P., Airoldi, A., Sala, G., Landro, L.D., Ruzzene, M., Spadoni, A., 2010, "Composite chiral structures for morphing airfoils: numerical analyses and development of a manufacturing process," Compos. B Eng., **41**, 133–147.
12- Martin, J., Heyder-Bruckner, J.J., Remillat, C., Scarpa, F., Potter, K., Ruzzene, M., 2008, "The hexachiral prismatic wingbox concept," Phys. Status Solidi B., **245**, 570–577.
13- Lim, T.C., 2015. Auxetic Materials and Structures. Springer, Singapore.
14- Prall, D., Lakes, R., 1996, "Properties of a chiral honeycomb with a Poisson's ratio of -1," Int. J. Mech. Sci., **39**, 305–314.
15- Scarpa, F., Blain, S., Lew, T., Perrott, D., Ruzzene, M., Yates, J., 2007, "Elastic buckling of hexagonal chiral cell honeycombs," Compos. A Appl. Sci. Manuf., **38**, 280–289.
16- Spadoni, A., Ruzzene, M., Scarpa, F., 2005, " Global and local linear buckling behavior of a chiral cellular structure," Phys. Status Solidi, **242**, 695–709
17- Grima, J.N., 2000, New auxetic materials. Ph.D. Thesis, University of Exeter.
18- Ma, Y., Scarpa, F., Zhang, D., Zhu, B., Chen, L., Hong, J., 2013, "A nonlinear auxetic structural vibration damper with metal rubber particles,"Smart Materials and Structures, 22, 084012.
19- Lim, T.C. 2002. ''Functionally Graded Beam for Attaining Poisson curving,'' Journal of Materials Science Letters, 21,1899-1901
20- Scarpa F., and Tomlinson, G., 2000, ''Theoretical characteristics of the vibration of sandwich plates with in-plane negative Poisson's ratio values,'' Journal of Sound and Vibration, **230**(1), 45-67.
21- Scarpa, F.L., Dallocchio, F., and Ruzzene, M., 2003, ''Identification of acoustic properties of auxetic foams,'' Proceedings of the SPIE 5052, 468-474.
22- Lira, C., Scarpa, F., Rajasekaran, R., 2011, "A gradient cellular core for aeroengine fan blades on auxetic configuration," J. Intelligent Mat. Sys. and Struct., **22**, 907-917.
23- Hou, Y., Tai, Y.H., Lira, C., Scarpa, F., Yates, J.R., Gu, B., 2013, "The bending and failure of sandwich structures with auxetic gradient cellular cores,". Composites Part A: Applied Science and Manufacturing, **49**, 119-131.

24- Maruszewski, B.T., Drzewiecki, A., and Starosta, R., 2013, ‘‘Thermoelastic damping in an auxetic rectangular plate with thermal relaxation—free vibrations,’’ Smart Materials and Structures, **22**(8), 084003.
25- Lim, T.C., 2014, ‘‘Buckling and vibration of circular auxetic plates,’’ Journal of Engineering Materials and Technology, **136**(2), 021007.
26- Ruzzene, M., Mazzarella, L., Tsopleas, P., Scarpa, F., 2002, "Wave Propagation in sandwich plates with periodic Auxetic core," J. Intelligent Mat. Sys. and Struct., **13**(9), 587-597.
27- Airoldi, A., Bettini, P., Panichelli, P., Oktem, M.F., and Giuseppe, S., 2015, ‘‘Chiral topologies for composite morphing structures – Part I: Development of a chiral rib for deformable airfoils,’’ Physica Status Solidi B, **252**(7): 1435-1445.
28- Shiyin, X., Xiuchang, H., Hongxing, H., 2014, "A study on the isolation performance of trichiral lattices with gradient geometry," J. Vib. and Cont., DOI:1077546314524261
29- Marburg, St., 2002, "Developments in Structural–Acoustic Optimization for Passive Noise Control," A of Computational Meth. in Eng. State of the art reviews, **9**, 291–370.
30- Chen, Y. J., Scarpa, F., Liu, Y. J., Leng, J. S., 2013, "Elastisity of anti-tetrachiral anisotropic lattices," Int. J. Solid and Struct., **50**, 996-1004
31- Lorato, A., Innocenti, P., Scarpa, F., Alderson, A., Alderson, K. L., Zied, K. M., Ravirala, N., Miller, W., 2010, "The transverse elastic properties of chiral honeycombs," Composite science and technology, **70**, 1057–1063.
32- ANSYS® Academic Research, Release 14.0, ANSYS, Inc.
33- Chekkal, I., Bianchi, M, Remillat, C., Bécot, F.-X., Jaouen, L., Scarpa, F., 2010, "Vibro-Acoustic Properties of Auxetic Open Cell Foam: Model and Experimental Results," ACTA ACUSTICA UNITED WITH ACUSTICA, 96, 266 – 274.
34- Petyt, M., 1990, Introduction to finite element vibration analysis, Cambridge University Press, Cambridge.
35- Ranjbar, M., Marburg, St., Hardtke, H.-J., 2012, "Structural acoustic optimization of rectangular plate: A tabu search approach," J. of finite element in analysis and design, **50**, 142-146.
36- Kollmann, F. G., 2000, Maschinenakustik-grundlagen, meβtechnik, berechnung, beeinflussung. (in German), 2nd revised edition, Springer-Verlag, Berlin, Heidelberg.
37- Fritze, D., Marburg, St., Hardtke, H.-J., 2009, "Estimation of Radiated Sound Power: A Case Study on Common Approximation Methods," Acta Acustica United With Acoustica, **95**, 833–842.
38- Ranjbar, M., Hardtke, H.-J., Fritze, D., Marburg, St., 2010, "Finding the best design within limited time: a comparative case study on methods for optimization in structural acoustics," J. Comput. Acoust., **18**, 149–164.